The MEXICO rotor aerodynamic loads prediction

ZigZag tape effects and laminar-turbulent transition modeling in CFD

Zhang, Ye; van Zuijlen, Alexander; van Bussel, Gerard

DOI
10.1016/j.jweia.2017.06.002

Publication date
2017

Document Version
Final published version

Published in
Journal of Wind Engineering & Industrial Aerodynamics

Journal of Wind Engineering & Industrial Aerodynamics 168 (2017) 152–163

Contents lists available at ScienceDirect

Journal of Wind Engineering & Industrial Aerodynamics

journal homepage: www.elsevier.com/locate/jweia

The MEXICO rotor aerodynamic loads prediction: ZigZag tape effects and laminar-turbulent transition modeling in CFD

Ye Zhang *, Alexander van Zuijlen, Gerard van Bussel

DUWIND, Faculty of Aerospace Engineering, TUDelft, Kluyverweg 1, 2629HS, Delft, The Netherlands

ARTICLE INFO

2010 MSC:
00-01
99-00

Keywords:
Tip loads overprediction
ZigZag tape effects
Laminar-turbulent transition
OpenFOAM
Wind turbine rotor simulation

ABSTRACT

This paper aims to provide an explanation for the overprediction of aerodynamic loads by CFD compared to experiments for the MEXICO wind turbine rotor and improve the CFD prediction by considering laminar-turbulent transition modeling. Large deviations between CFD results and experimental measurements are observed in terms of sectional normal and tangential forces at the blade tip ($r/R = 0.82$ and 0.92) of the MEXICO rotor operating in axial condition at the design tip speed ratio $\lambda = 6.7$. The first part of this study identifies the effects of ZigZag tape, which is used in the experiment to trigger boundary layer transition, by analyzing the available experimental data of a single, non-rotating MEXICO rotor blade. The analysis indicates that ZigZag tape has a significant impact on sectional aerodynamic tip loads: it alters the boundary layer thickness and additionally reduces the effective airfoil camber besides the expected tripping. These additional effects most likely also occur in the rotating MEXICO experiment, reducing the sectional loads and hence lead to an overprediction by CFD. To eliminate the ZigZag tape interference, experimental data with an untripped blade is preferred to be used as validation case. In the second part of this study, a transitional flow simulation for the MEXICO rotor is performed by using RANS-based transition model $k-k_L-\omega$ within OpenFOAM-2.1.1. The numerical results are compared against experimental data obtained from the untripped, new MEXICO experiments. The comparison gives that transitional simulation present a very good tip loads prediction for the untripped blade. The measured data also confirms that the ZigZag tape indeed has a significant influence on the blade tip loads in rotating conditions. The transition onset over 3D MEXICO blade is visualized and transition locations are identified. The results shown in the present study can explain the causes of the large differences between CFD and experiment observed in the MEXICO blind comparisons.

1. Introduction

Accurate aerodynamic loads prediction on wind turbine blades is important for turbine design. It is crucial not only for power output estimation, but also for wind turbine blade lifetime prediction. Therefore, in the last two decades, several representative wind tunnel measurements (Hand et al., 2001; Snel et al., 2007) were carried out to provide high quality experimental data for validating and improving aerodynamic models. One of such measurements is the MEXICO (Model EXperiments In Controlled cOnditions) experiment, which measured a three-bladed wind turbine model with $4.5m$ diameter in the $8 \times 6m^2$ open test section of DNW-LLF (German-Dutch Wind Tunnel-Large Low-speed Facility) wind tunnel.

Blind comparisons of aerodynamic loads predictions with plenty of different aerodynamic models, including lifting line codes and CFD codes from different project partners were performed. The comparisons showed that the numerical results significantly overpredict the aerodynamic tip loads compared to the measurements, even with high fidelity RANS-based CFD codes (Schepers et al., 2014). Fig. 1 shows the comparison of normal force distribution along the blade between predicted results from different CFD codes and experimental data (Schepers et al., 2014). The tip speed ratio is $\lambda = 6.7$, which is the optimal design case. The flow over the blade should be mostly attached. From the comparison it can be seen that almost all CFD RANS simulations significantly overpredict the normal force at radial locations $r/R = 0.82$ and 0.92. For the tangential force, the comparison becomes even worse than the normal force at these locations, which is shown in Fig. 2. Although it has been known that wind tunnel effects and tunnel calibration issues in MEXICO experiment could be possible causes of the discrepancies between CFD and the experimental results, the reason for the large overprediction is

* Corresponding author.
E-mail address: ye.zhang@tudelft.nl (Y. Zhang).

http://dx.doi.org/10.1016/j.jweia.2017.06.002
Received 5 December 2016; Received in revised form 2 June 2017; Accepted 11 June 2017

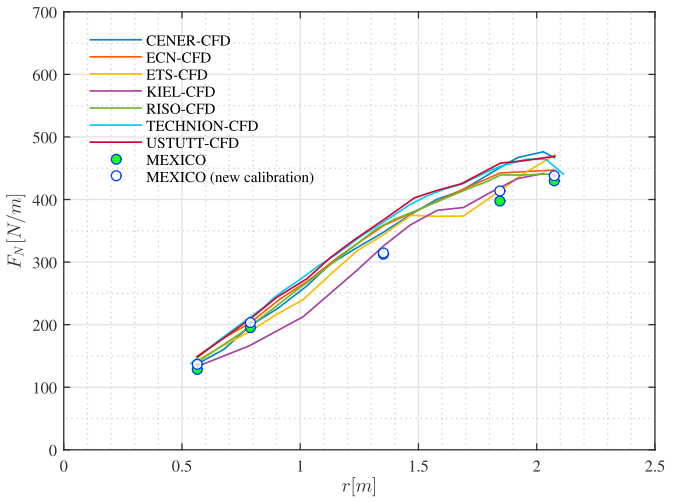

Fig. 1. Comparison of normal force distribution along the blade between CFD predictions and MEXICO measurement for the design condition: $\lambda = 6.7$, $U_\infty = 15m/s$, $n = 424.5rpm$. The data of new MEXICO measurement which includes latest calibrations (tunnel speed and pressure sensor) is also added. The approximate differences in measured conditions between two experiments are $\Delta U_\infty = 0.1m/s$, $\Delta n = 0.6rpm$.

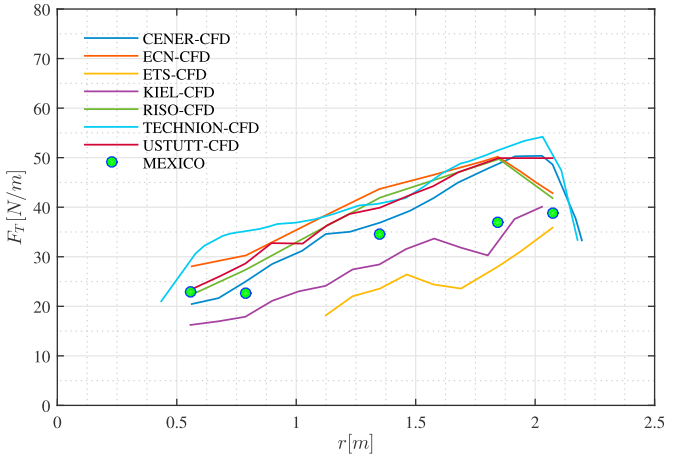

Fig. 2. Comparison of tangential force distribution along the blade between CFD predictions and measurement, $\lambda = 6.7$, $U_\infty = 15m/s$, $n = 424.5rpm$.

still not fully understood yet. The data of the new MEXICO experiment including latest calibration (tunnel speed and pressure sensor) is also shown in Fig. 1. These data show that with the new calibration, a slightly higher sectional load is measured, but that the CFD codes still significantly overpredict the outboard sectional loads.

It is well known that RANS modeling is capable of predicting attached flow quite well. The comprehensive overprediction shown above could not be originated from numerical modeling failure. The remaining possibility could be the CFD geometry deviations from the measured model in the wind tunnel. Indeed, the largest difference between experiment and CFD computation is that in the experiment the boundary layer is tripped by using ZigZag tape on both pressure side and suction side of the blade to trigger the flow fully turbulent. It is assumed that the ZigZag tape only effects the flow by promoting transition from laminar to turbulent. However, it is very challenging for CFD to model and mesh the exact ZigZag tape geometry and consequently the boundary layer is modeled as fully turbulent over the whole blade in the simulations. Instead, the effects of the ZigZag tape on blade loads have not been discussed and fully turbulent flow simulations on clean blade without the ZigZag tape are assumed in almost all calculations except for the ETS code which solves laminar flow over the blade. This assumption can be found in many studies (Bechmann et al., 2011; Tsalicoglou et al., 2014; Plaza et al., 2015).

Regarding the ZigZag tape effects on 2D airfoil aerodynamic characteristics (Selig, 1995), discussed the effects of ZigZag tape width, height and trip location on airfoil performance for two specific sailplane airfoils: E374 and SD7037. For wind turbine airfoils (Van Rooij and Timmer, 2003), discussed the ZigZag tape effects on the momentum thickness of the turbulent boundary layer. The comparisons of airfoil performance between clean and rough configurations are also shown for several 2D thick airfoil classes. Van Rooij and Timmer (2003) concludes that an effective ZigZag tape will lead to a significant increase in momentum thickness of the turbulent boundary layer and sometimes will reduce (the maximum) lift. The height of distributed roughness k is determined according to the method mentioned in the paper (Braslow and Knox, 1958). Moreover, critical roughness Reynolds number ($R_k = \frac{u_k k}{\nu_k}$), based on the roughness height k and the local flow conditions in the boundary layer at the top of the roughness, plays a role as well. The required roughness height is reduced when the undisturbed air velocity increases (Van Rooij and Timmer, 2003).

Therefore, the present paper aims to investigate the ZigZag tape effects on the measured sectional loads by the analysis of available experimental data in the non-rotating MEXICO experiment. Eventually, the objective of this study is to identify the cause of large deviation in the blade tip loads comparison and to improve the prediction of CFD results for the MEXICO rotor. This paper is organized as follows: Section 2 presents the brief description of the non-rotating experiment and the analysis of ZigZag tape effects with measured data. Section 3 introduces the numerical models for simulating the transitional flow over the MEXICO rotor. Section 4 describes the computational setup, grid generation and boundary conditions. Results and discussion will be shown afterwards in Section 5. Finally, the conclusions will be drawn in Section 6.

2. The non-rotating MEXICO experiment and ZigZag tape effects

The non-rotating MEXICO experiments were carried out in the low speed low turbulence wind tunnel at Delft University of Technology (TUDelft) in November 2013 (Zhang et al. ; Boorsma and Schepers, 2014). This measurement campaign is an intermediate step before the new rotating MEXICO experiment in phase II. In the non-rotating measurement, the sectional airfoil aerodynamic characteristics of the MEXICO blade with two different configurations are measured. One configuration is the clean blade without any roughness, the other configuration is blade with ZigZag tape roughness. Fig. 3 illustrates the shape and critical parameters of the ZigZag tape. The ZigZag tape used in the non-rotating experiment is almost the same as in the previous rotating measurement. The operating conditions and the ZigZag tape parameters are listed in Table 1. The DU91-W2-250 airfoil at $r/R = 0.35$ and the NACA64-618 airfoil at $r/R = 0.92$ radial locations are measured with Kulite pressure sensors for different angles of attack. The chord-based Reynolds number is about $Re_c = 0.5 \times 10^6$. The experimental

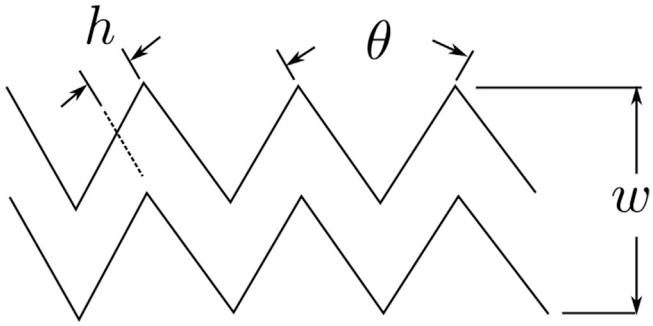

Fig. 3. The shape and critical parameters of ZigZag tape.

Table 1
The operating condition in the non-rotating experiment and parameters of ZigZag tape applied on the blade.

Inflow speed U_∞ $[m/s]$	60	ZigZag tape length r/R [−]	$0 \sim 0.95$
Turbulence intensity Tu [%]	0.06	ZigZag tape height h [mm]	0.20
Geometric angle of attack α [°]	$-20^\circ \sim 20^\circ$	ZigZag tape width w [mm]	10
Chord-based Reynolds number Re_c [−]	$\sim 0.5 \times 10^6$	ZigZag tape angle θ [°]	60

setup is shown in Fig. 4. Detailed experiment description can be found in the reference (Zhang et al.). Apart from the measurement, a RANS simulation of fully turbulent flow over the non-rotating blades with the $k-\omega$ *SST* turbulence model has been performed in order to compare against the wind tunnel measurements, which is also referred in the work (Zhang et al.).

2.1. ZigZag tape effects on measured local pressure distribution C_p

Fig. 5 presents the results of measured pressure distribution at radial location $r/R = 0.92$ for three different angles of attack: $\alpha = 8^\circ, 10^\circ$ and 16°. The blade with ZigZag tape acquires lower pressure on the pressure side than clean blade. On the other hand, on the suction side, obviously more pressure suction is obtained with the clean blade configuration, resulting in much lower pressure near the leading edge. This lower pressure occurs in the regions $x/c = 0 \sim 0.30$ and $x/c = 0.40 \sim 0.70$, respectively. After $x/c = 0.70$, conversely a bit higher pressure is observed on the clean blade near the trailing edge. When the angle of attack increases, the ZigZag tape effects seem to play a less important role in the local pressure distribution.

2.1.1. ZigZag tape effects on measured integrated force c_l and c_d

Fig. 6 presents the comparisons of c_l and c_d polar for the clean and tripped blades at $r/R = 0.92$ radial location. The airfoil profile at this section is NACA64-418. The ZigZag tape plays a significant role in reducing the lift force in particular flow regimes, which is when $\alpha = 4^\circ \sim 11^\circ$. However, at attached flow condition where $\alpha < 4^\circ$, the ZigZag tape has little influence on lift reduction. The same effect is observed at higher angle of attack $\alpha > 11^\circ$ as well. Meanwhile, the drag force is not influenced by the ZigZag tape significantly when the angle of attack is larger than 10°. But considerably higher drag force is obtained with tripped blade when α is below 10°, and the largest difference in drag force between clean and tripped blade appears at $\alpha = 8^\circ$.

2.1.2. Estimated ZigZag tape effects on CFD numerical results

Fig. 7 shows the comparison of local chordwide pressure distribution at $r/R = 0.92$ between experimental measurement and CFD result at $\alpha = 8^\circ$ (Zhang et al., 2014). From the C_p comparison, it can be observed that 3D CFD result with fully turbulent simulation has closer C_p agreement with the clean blade measurement in the region $x/c = 0.05 \sim 0.80$, rather than with the blade with ZigZag tape roughness. Since the aim of attaching ZigZag tape is to trigger only the flow to fully turbulent, the fully turbulent condition in the experiment with tripped blade was believed much easier in order to validate a numerical code in terms of modeling such as CFD codes, in which fully turbulent assumption is generally applied. However, the C_p comparison shows a clear proof that the ZigZag tape has a significant influence on the C_p prediction. The existence of ZigZag tape clearly alters the airfoil boundary layer displacement thickness and decambers the airfoil.

Fig. 8 plots the 92%*R* sectional normal force comparisons by integrating the experimental and numerical pressure at the same chordwise locations. Similarly to the pressure distribution comparison, the normal force for the clean blade is much larger than for the tripped blade, as expected. The difference is about $7\%F_{N_{rough}}$. Due to the ZigZag tape effects, a significant overprediction is observed for the fully turbulent CFD simulation compared to results of the tripped blade. However, almost the same normal force is predicted by CFD for the clean blade. In other words, fully turbulent CFD simulation overpredicts the sectional normal force on the blade with ZigZag tape, because the ZigZag tape alters the boundary layer displacement thickness and airfoil camber.

The question that needs to be answered here is whether the difference in C_p distribution discussed above between clean blade and tripped blade

Fig. 4. Two experimental setups for the non-rotating MEXICO blade measurement in the low speed low turbulence wind tunnel of Delft University of Technology.

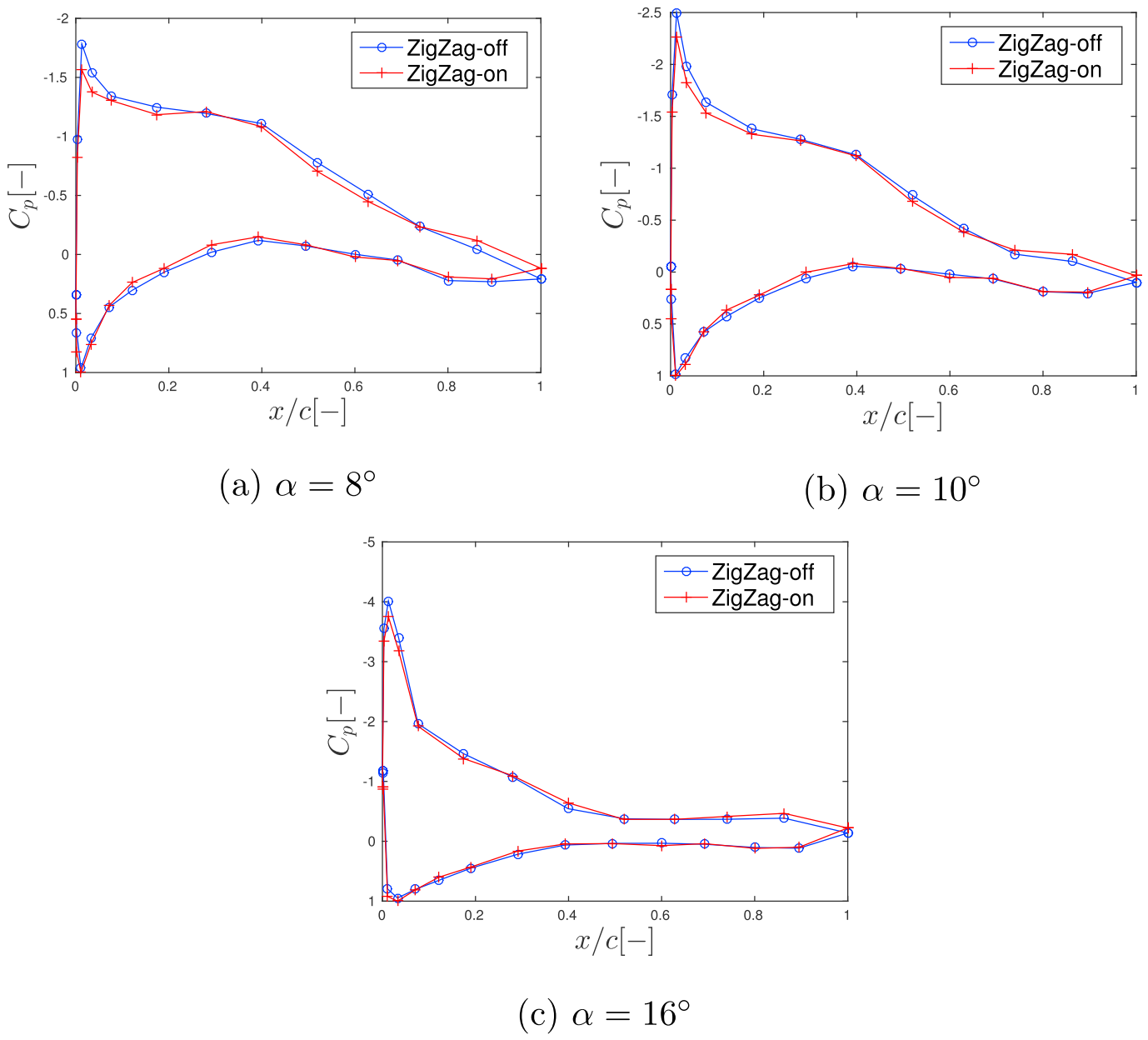

Fig. 5. The effects of ZigZag tape on local pressure distribution in the experiment. C_p comparison with and without ZigZag tape at $r/R = 0.92$ radial location, $\alpha = 8°$, $10°$ and $16°$.

is an expected result when the boundary layer is tripped or that it is more than expected. Figs. 9 and 10 further demonstrate the hypothesis that the applied ZigZag tape not only plays a role in triggering flow transition at specific location, but has greater effect than that. The numerical results shown in these figures are obtained from *Rfoil* (Van Rooij), which is based on a viscous-inviscid method for wind turbine airfoil analysis. Fig. 9 clearly demonstrates that *Rfoil* presents very good capability for predicting C_p distribution for the clean 2D NACA64-418 airfoil. However, there are notable differences observed both on the suction side and pressure side between numerical result and experimental measurement for the tripped 2D NACA64-418 airfoil in Fig. 10. The transition locations on the suction and pressure sides in *Rfoil* calculation are specified as the experiment, but without any roughness height. The amplification factor $N = 9$ is used in the transition model e^N for the *Rfoil* computation due to the very low turbulence level in wind tunnel. As it can be seen from the comparison, the measured pressure on the suction side with ZigZag tape height of $0.2mm$ presents considerably less pressure suction compared to *Rfoil* results, particularly in the region $x/c = 0 \sim 0.8$. The ZigZag tape on the pressure side shows less influence on the pressure, even if the ZigZag tape height of $0.32mm$ is larger than the one used on the suction side. To quantitatively state the extra effects caused by ZigZag tape, the experimental result produces 5.7% lower c_l and 10% higher c_d compared to numerical result without any roughness height. These extra "negative" effects indicate that the ZigZag tape, as an intrusive device to trigger transition, significantly affects and disturbs the local flow over the airfoil and further the aerodynamic loads due to its explicit existence. The consequence of attaching ZigZag tape with same height on the rotating blade tip $r/R = 0.92$ could be more severe than the difference in C_p on the suction side shown in Fig. 10, because the ratio of ZigZag tape height to local chord length (h/c) in the rotating blade case is larger than the 2D airfoil case. The effect of ZigZag tape is a possible explanation for the aerodynamic loads overprediction by CFD.

The ZigZag tape effects discussed above are not taken into account by any CFD simulations for the MEXICO rotor. This observation can explain why almost all CFD results in the rotating MEXICO experiment consistently overestimate the normal force near the blade tip, even through the

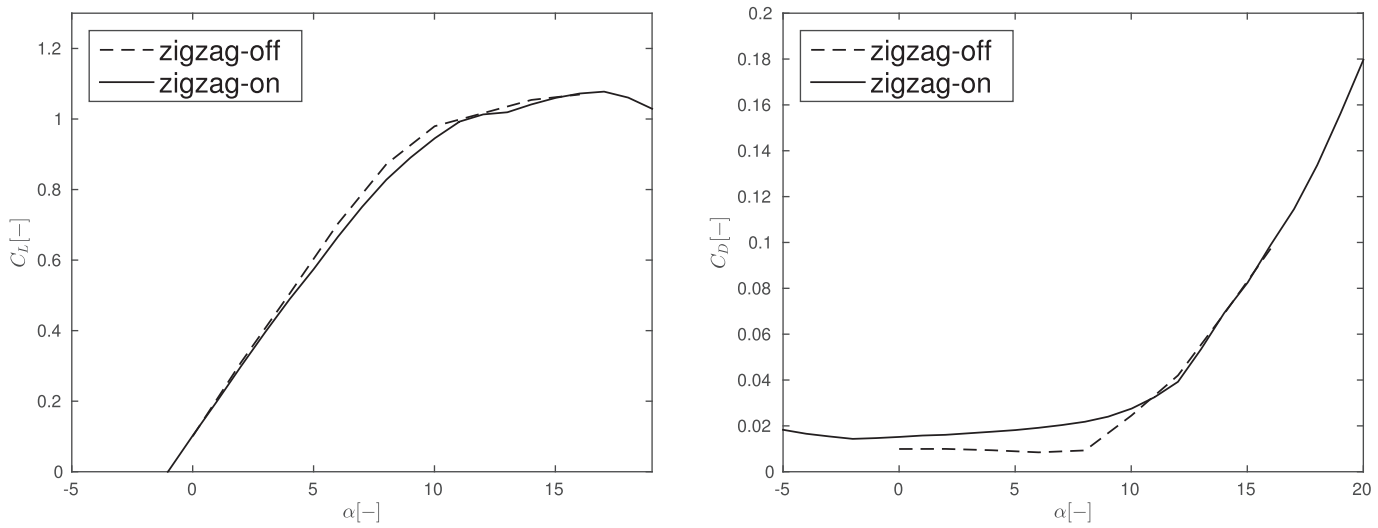

Fig. 6. The effects of ZigZag tape on the integrated lift c_l and drag c_d polar of NACA64-418 airfoil at radial location $r/R = 0.92$.

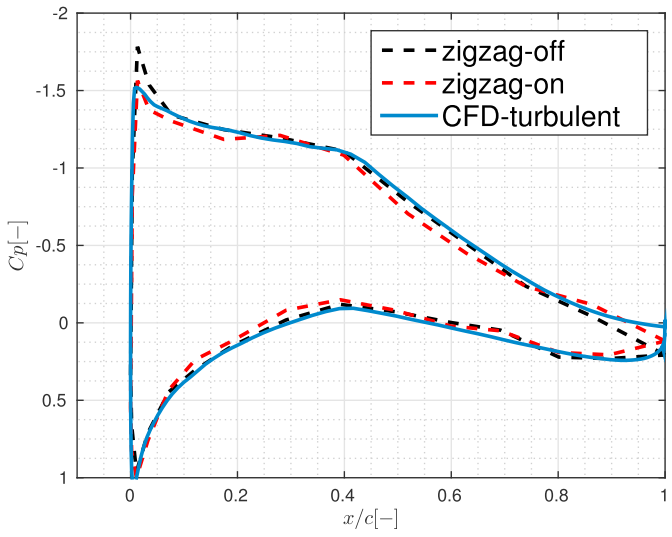

Fig. 7. The influence of ZigZag tape on the local pressure distribution. C_p comparison with and without ZigZag tape and CFD prediction at $r/R = 0.92$, $\alpha = 8^{\circ}$.

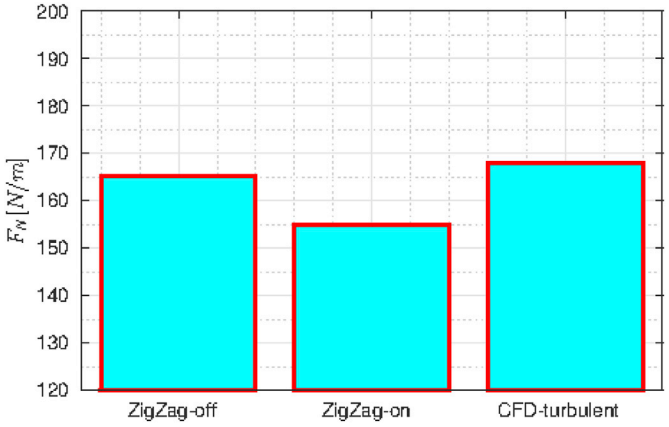

Fig. 8. The results of integrated sectional normal force at $r/R = 0.92$ with angle of attack $\alpha = 8^{\circ}$.

rotor is operating at the design tip speed ratio. From the c_l and c_d curves shown in Fig. 6, one can conclude that the lift and drag forces influenced mostly by the existence of ZigZag tape roughness are at an angle of attack α in the range from 4° to 11°. When $\lambda = 6.7$, the effective angle of attack estimated at $r/R = 0.82$ and 0.92 on the rotating blade are just in this region (7.3° ∼ 8.4° as estimated by BEM code), and consequently the ZigZag tape on the rotating blade most likely shows similar or even stronger effects on the aerodynamic loads as observed in the non-rotating experiment.

According to the above analysis, it can be concluded that the existence of ZigZag tape has a significant impact on the sectional loads and decambers the airfoil. Therefore, it is recommended to exclude these effects from measured results. For that reason, in the new MEXICO experiment carried out in July 2014, the aerodynamic loads were measured with clean blade configuration (Boorsma and Schepers, 2014, 2015). Without tripped boundary layer, transitional flow from laminar to turbulent has to be considered in CFD simulation. The following section briefly describes the $k-k_L-\omega$ transition model used in the present study and validates it with two test cases before utilizing it for the complicated 3D rotating wind turbine case.

3. Transition model

3.1. Laminar-turbulent transition modeling

The present $k-k_L-\omega$ transition model is based on the low-Re $k-\omega$ shear stress transport (SST) eddy-viscosity model. Compared to other RANS-based transition models, such as $\gamma-Re_\theta$ SST, the advantage of the present model is the elimination of the intermittency factor, a semi-empirical parameter bridging the pre-transitional and turbulent boundary layer and to enforce transition onset (Walters and Leylek, 2002). The $k-k_L-\omega$ model is a three-equation model, the transport equation of laminar kinetic energy k_L is added to model the low frequency velocity fluctuations. The transport equations for the turbulent kinetic energy k_T, the laminar kinetic energy k_L and the specific dissipation rate ω in incompressible form are written below:

$$\frac{Dk_T}{Dt} = \underbrace{P_{k_T}}_{\text{production}} + \underbrace{R_{BP} + R_{NAT}}_{\text{bypass and natural transition}} - \underbrace{\omega k_T}_{\text{destruction}} - \underbrace{D_T}_{\text{anisotropic dissipation}} + \underbrace{\frac{\partial}{\partial x_j}\left[\left(\nu + \frac{\alpha_T}{\sigma_k}\right)\frac{\partial k_T}{\partial xj}\right]}_{\text{diffusion}} \tag{1}$$

$$\frac{Dk_L}{Dt} = \underbrace{P_{k_L}}_{\text{production}} \underbrace{-R_{BP} - R_{NAT}}_{\text{bypass and natural transition}} - \underbrace{D_L}_{\text{anisotropic dissipation}} + \underbrace{\frac{\partial}{\partial x_j}\left[\nu\frac{\partial k_L}{\partial x_j}\right]}_{\text{diffusion}} \tag{2}$$

$$\frac{D\omega}{Dt} = \underbrace{C_{\omega 1}\frac{\omega}{k_T}P_{k_T}}_{\text{production}} + \underbrace{\left(\frac{C_{\omega R}}{f_W} - 1\right)\frac{\omega}{k_T}(R_{BP} + R_{NAT})}_{\text{bypass and natural transition}} - \underbrace{C_{\omega 2}f_W^2\omega^2}_{\text{destruction}} + \underbrace{C_{\omega 3}f_\omega\alpha_T f_W^2\frac{\sqrt{k_T}}{d^3}}_{\text{boundary layer wake correction}} + \underbrace{\frac{\partial}{\partial x_j}\left[\left(\nu + \frac{\alpha_T}{\sigma_\omega}\right)\frac{\partial\omega}{\partial x_j}\right]}_{\text{diffusion}} \tag{3}$$

3.2. Implementation and validation of the transition model

The first version of OpenFOAM which includes the three transport equation $k-k_L-\omega$ transition model is OpenFOAM-2.1.1. Unfortunately, there are some implementation errors found in the source code. The model used in this study is the revised model which is implemented in OpenFOAM-2.1.1 based on the paper (Fürst et al., 2013). The revised model is named "corrected kkLOmega" in this paper and verification of this model implementation and validation of its capability are shown below.

First of all, the test case of 2D channel flow is tested for the $k-k_L-\omega$ transition model to verify the code. The friction Reynolds number is $Re_\tau = 395$ based on the half channel height δ, $Re_\tau = \frac{u_\tau\delta}{\nu}$. The DNS data of (Moser et al., 1999) is used to compare the predicted mean velocity profile and total fluctuation kinetic energy of $k-k_L-\omega$ transition model. In terms of the total fluctuation kinetic energy $k = \frac{1}{2}(u'u' + v'v' + w'w')$, which corresponds to the $k_{TOT} = k_T + k_L$ within the transition model, the comparison in Fig. 11a shows that the fluctuation in the outer layer significantly overpredicted by the wrong implementation. The correctly implemented model in OpenFOAM-2.1.1 gives reasonable results, but with a slight overprediction of total fluctuation kinetic energy in the regions $10 < y^+ < 50$ and $y^+ > 300$.

The simulations of flow over 2D wind turbine airfoil DU91-W2-250 are carried out to evaluate the performance of transition model $k-k_L-\omega$ with respect to transition onset. The chord-based Reynolds number is $Re_c = 1.0 \times 10^6$. A fully structured O-type grid is used for the CFD simulations. The computational domain is about 100 chord in order to reduce the influence of the boundary. The turbulence intensity is 0.06% in all these simulations. The numerical results of turbulent reattachment point for a range of angles of attack are compared with experimental measurement of TUDelft, since in the experiment the microphone is used to detect the transition onset location, where turbulent reattachment point is close to. Fig. 11b shows the comparison of transition onset locations on the suction surface of DU91-W2-250 airfoil at $Re_c = 1.0 \times 10^6$. The numerical prediction of turbulent reattachment point has a good agreement with measured data for a large range of angles of attack. Only at $\alpha = 9.24^\circ$ the turbulent reattachment prediction is delayed compare to the experiment.

The revised version of the $k-k_L-\omega$ transition model in OpenFOAM-2.1.1 is considered correctly implemented and it presents good performance of transition onset prediction for the 2D wind turbine airfoil. The numerical setup of transitional flow simulation for the 3D MEXICO wind turbine rotor with $k-k_L-\omega$ model is described in the following section.

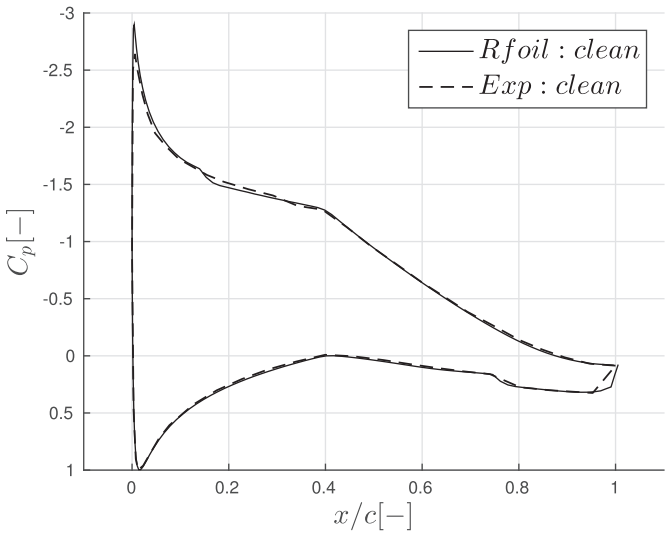

Fig. 9. The comparision of pressure distribution between *Rfoil* and experiment for the clean NACA64-418 airfoil. The Reynolds number is $Re = 0.7 \times 10^6$ and the geometric angle of attack is $\alpha = 8^\circ$. It demonstrates that *Rfoil* presents good capability for predicting C_p distribution.

4. Grid generation and boundary conditions

The geometry of the MEXICO rotor and simulated condition is shown

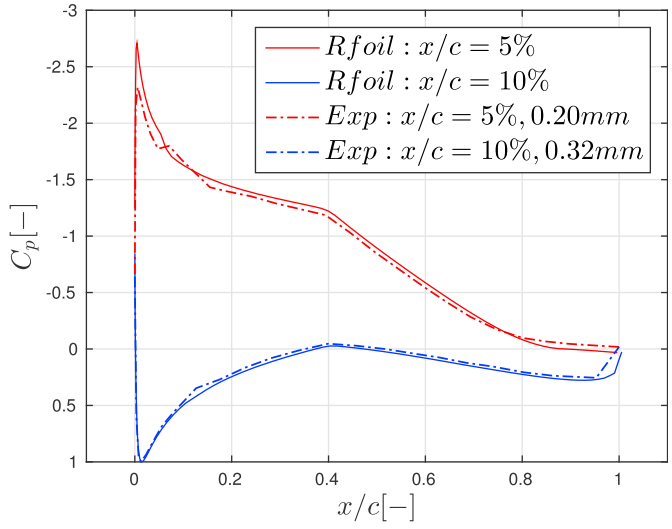

Fig. 10. The comparision of pressure distribution between *Rfoil* and experiment for the rough NACA64-418 airfoil tripped by ZigZag tape. The Reynolds number is $Re = 0.7 \times 10^6$ and the geometric angle of attack is $\alpha = 8^\circ$. The configurations of ZigZag tape are: at suction side $x/c = 5\%$ with ZigZag tape height of 0.2*mm* and at pressure side $x/c = 10\%$ with ZigZag tape height of 0.32*mm*.

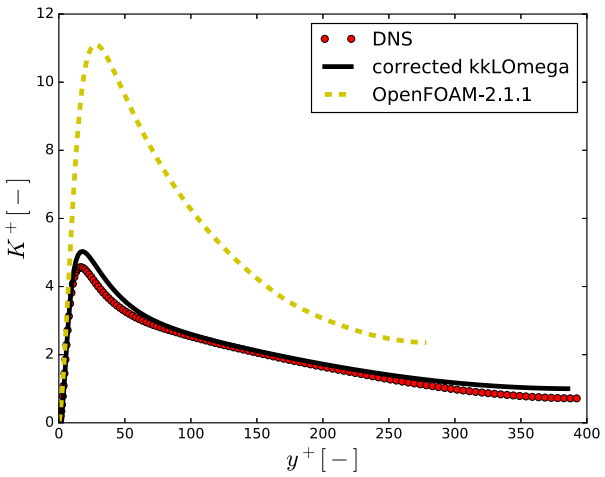

(a) Comparison of total fluctuation kinetic energy ($k_{TOT} = k_T + k_L$) for the channel flow, normalized by the friction velocity.

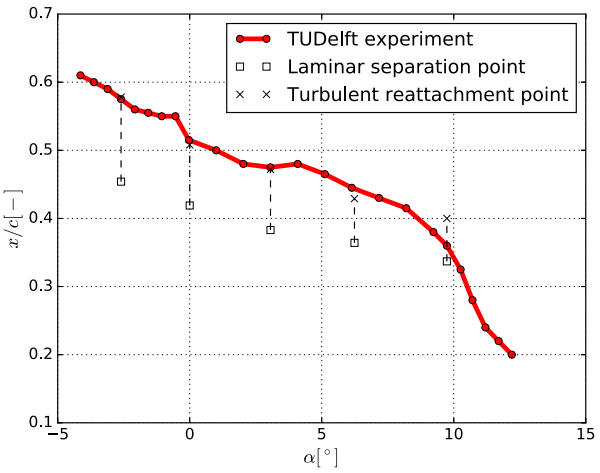

(b) Transition onset prediction for DU91-W2-250 wind turbine airfoil for different angles of attack at $Re_c = 1.0 \times 10^6$, $Tu = 0.06\%$

Fig. 11. Verification and validation of implemented $k-k_L-\omega$ transition model in OpenFOAM-2.1.1.

Table 2
Blade geometry and simulated conditions.

Number of blades $B[-]$	3	Rotational speed $n[rpm]$	425.1
Rotor radius $R[m]$	2.25	Free-steam velocity $U_\infty[m/s]$	15.03
Hub radius $r_{hub}[m]$	0.21	Tip speed ratio $\lambda[-]$	6.7
Twist angle at $r/R = 0.20[^\circ]$	16.4	Tip Reynolds number $Re_{tip}[-]$	0.76×10^6
Turbulence intensity $Tu[\%]$	0.8	Pitch angle [°]	− 2.3

Table 3
The characteristics of three different levels of blade grids.

Grid Characteristic	Coarse	Medium	Fine
Chordwise nodes	80	120	160
Spanwise nodes	225	225	225
First grid spacing (mm)	0.015	0.006	0.004
Maximum y^+	< 1	< 0.5	< 0.35
Maximum skewness	3.00	1.652	2.65
Maximum orthogonality	78.8	79.2	80
Total cells	2.33×10^6	3.11×10^6	3.16×10^6

in Table 2. The computational domain is a one third of cylinder and rotor with periodic boundary in order to reduce the computational cost. A high quality multi-block O-type structured grid is generated near the blade surface by using hyperbolic method. A fixed growth rate of 1.1 is used for extruding the viscous boundary layer grid. By changing the first cell height normal to the blade surface and the number of nodes in the chordwise direction, the grid refinement study is achieved by using three different levels of grids. The detailed grid characteristics are listed in Table 3. The surface and volume meshes are illustrated in Figs. 13 and 14. Besides, the farfield grid is generated by using unstructured tetrahedral grid.

The CFD solver used is OpenFOAM-2.1.1 (Open Field Operation And Manipulation), an open source CFD code using the finite volume method. All the flow quantities are stored in the center of the discretized control volume using a collocated methodology. Rhie-Chow correction (Rhie and Chow, 1983) is used to remove the oscillations in the solutions when applying the collocated grid. The steady-state incompressible Reynolds-Averaged Navier-Stokes (RANS) equations are decoupled and solved with SIMPLE (Semi-Implicit Method for Pressure-Linked Equations) algorithm of Patankar and Spalding (1972). Multiple reference frame (MRF) approach is used to model the rotating flow by adding the Coriolis force in the momentum equations for the MRF zones. A second-order accurate linear-upwind scheme linear-upwind is used to discretize the convection term for velocity and a total variation diminishing (TVD) scheme based on central differencing with limiter is chosen for the convective terms k_T,k_L and ω. Diffusion terms are discretized with a second order centered scheme. Both the three equation transition model $k-k_L-\omega$ and the two equation fully turbulent model $k-\omega$ *SST* of (Menter and Esch, 2001) are used to investigate the transitional effects on the computed sectional aerodynamic loads on the blade.

The boundary condition at the inlet is Dirichlet for the inflow velocity and turbulent inflow variables, calculated as in (Walters and Leylek,

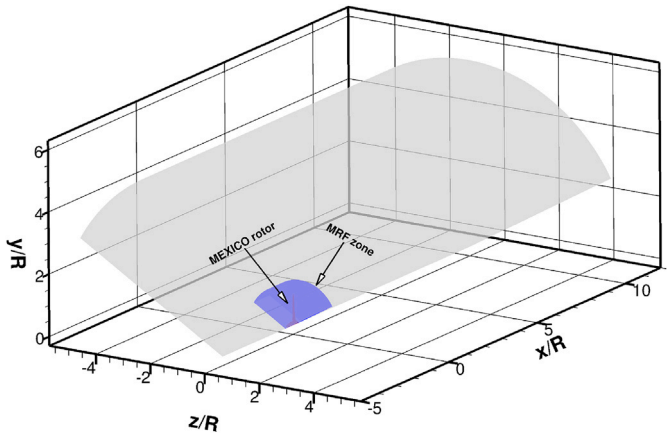

Fig. 12. Schematic view of the computational domain.

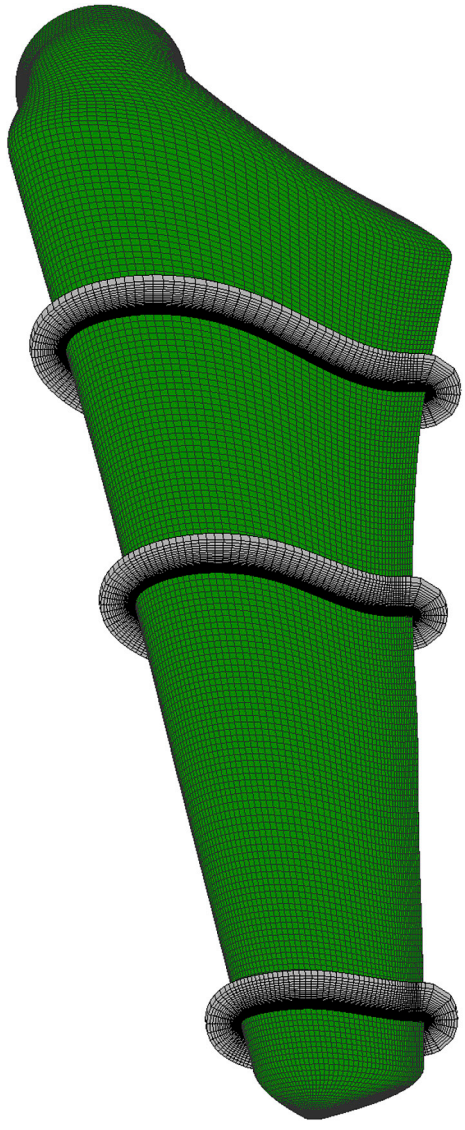

Fig. 13. Illustation of the boundary layer mesh along the blade.

2002), and a zero gradient Neumann boundary condition for the pressure. Zero gradient at the outlet for all variables, expect for the pressure for which a Dirichlet condition with a zero mean is imposed. Euler slip wall conditions are used at the hub surfaces, while no-slip wall boundary conditions are applied at the surfaces of rotor blades. Arbitrary mesh interface (AMI) technology (Farrell and Maddison, 2011) is imposed at the interfaces connecting the MRF rotating zone and stationary zone. Zero gradient is used for the farfield boundary of the computational domain. In particular, cyclic boundary conditions are enforced at the 120° periodic boundaries for the computational domain, see Fig. 12.

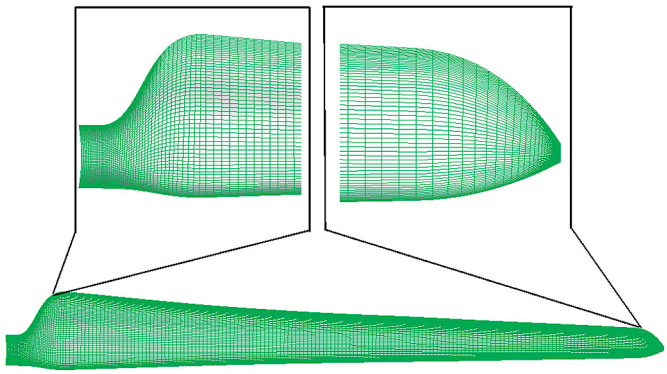

Fig. 14. Illustation of the surface mesh on the blade.

5. Results and discussion

In this section, firstly, grid independence and convergence studies are carried out on three grid levels. Then a simulation which features free transition along the full span is performed for the MEXICO rotor and the transitional effects on the sectional aerodynamic loads are discussed for $\lambda = 6.7$. The numerical loads prediction considering transitional flow is compared with the aerodynamic loads acquired in the new MEXICO experiment for the clean configuration. Only the outboard part ($r/R > 0.7$) of the blade (NACA profile) is clean, the rest part of the blade is still tripped in the experiment (Boorsma and Schepers, 2014, 2015). Finally, the computed transition lines are visualized on blade surfaces and transition onset locations are quantitatively identified.

5.1. Grid independence study and convergence study

In order to examine which grid is fine enough to discretize the domain of space, simulations are carried out on three grids with different densities as shown in Table 3 with the wind speed $U_\infty = 15.03m/s$ and tip speed ratio $\lambda = 6.7$. Fig. 15a plots the comparison of thrust on the rotor for these three cases. The difference between medium mesh and fine mesh is less than 1%. Meanwhile, the sectional pressure distribution and skin friction on three grids are further examined, showing almost the same results between the medium mesh and the fine mesh. Therefore, the medium mesh is considered sufficient for mesh independence. The results shown below are the numerical solutions obtained on the medium mesh.

In addition, the discretization schemes show good numerical stability and convergence, as can be seen in Fig. 15b. The final scaled residuals (Jasak et al.) of all conserved variables are below 10^{-4}. Taking the thrust iteration history into account, the numerical solution is considered fully converged.

5.2. Transitional effects

Figs. 16 and 17 compare the computed sectional, normal and tangential force distribution between transitional *corrected kkLOmega* and fully turbulent $k-\omega$ SST. It is shown that both F_N and F_T with considering boundary layer transition are higher than fully turbulent results. These observations are expected since when part of flow over the airfoil is laminar, generally more pressure suction is obtained on the

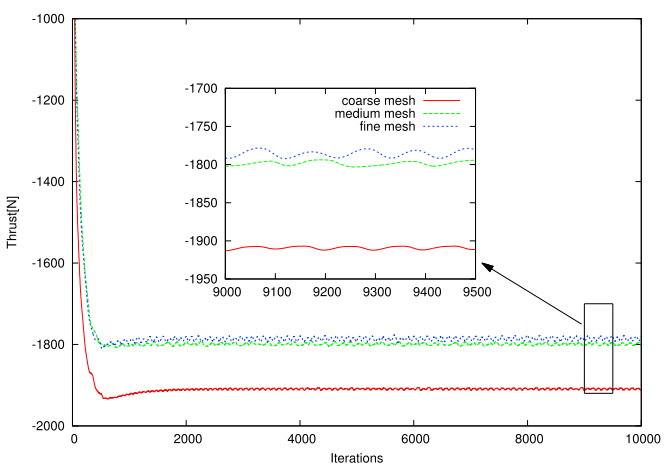

(a) Thrust convergence history.

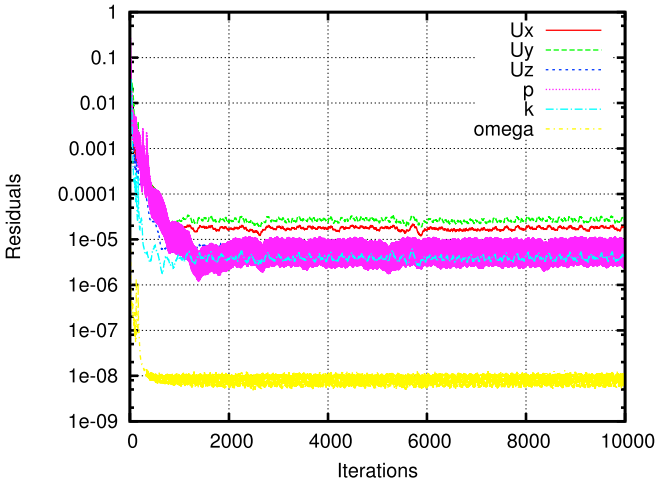

(b) Residuals convergence history.

Fig. 15. a) Comparison of thrust on the rotor with three different grids b) Residuals convergence history for conserved variables on the medium mesh.

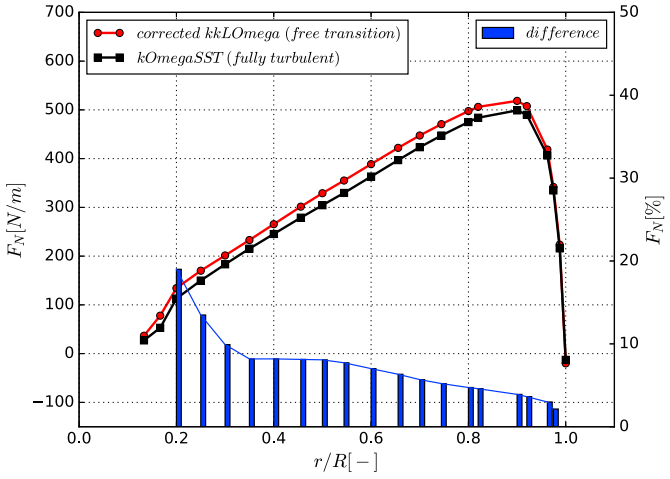

Fig. 16. Transitional effects on the normal force along the blade at design tip speed ratio $\lambda = 6.7$ ($U_\infty = 15.03m/s$, $n = 425.1rpm$, $\rho = 1.191kg/m^3$). The blue bar indicates the relative difference between two predictions. (For interpretation of the references to colour in this figure legend, the reader is referred to the web version of this article.)

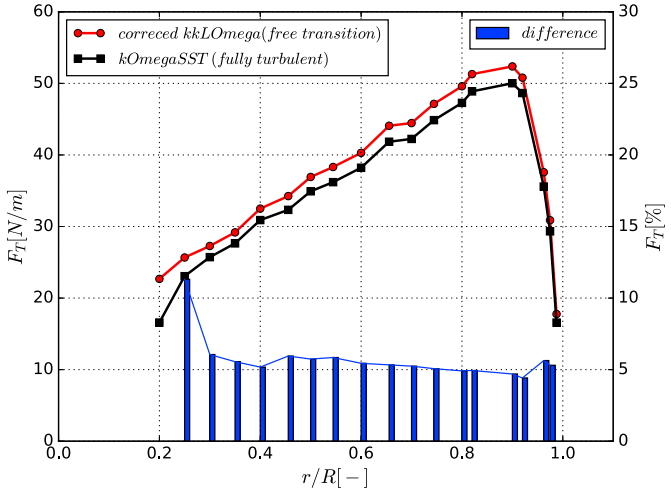

Fig. 17. Transitional effects on the tangential force (with viscous force) along the blade at design tip speed ratio $\lambda = 6.7$ ($U_\infty = 15.03m/s$, $n = 425.1rpm$, $\rho = 1.191kg/m^3$). The blue bar indicates the relative difference between two predictions. (For interpretation of the references to colour in this figure legend, the reader is referred to the web version of this article.)

upper surface. Figs. 18 and 19 show the more detailed information of sectional pressure distribution at $r/R = 0.35$ and $r/R = 0.92$ radial positions. Indeed, the main difference can only be found on the suction side. To quantify the difference in the forces, the relative difference is defined as $\frac{F_{transition} - F_{turbulent}}{F_{turbulent}}$. The relative difference in normal force is almost decreasing towards to the tip, which also indicates that transition has more influence at the inboard part of blade. Approximate 5% tangential force difference is observed for all the sections on the blade.

5.3. Aerodynamic loads prediction with the new MEXICO experiment

Fig. 20 compares the aerodynamic loads between the CFD transitional case, fully turbulent case, MEXICO experiment and new MEXICO experiment. The experimental wind speed for the MEXICO experiment shown in the figure was not corrected for the updated tunnel calibration. In the new MEXICO experiment, both configurations with and without ZigZag tape are measured, while in the MEXICO experiment only the tripped blade is measured. It can be clearly seen there are some differences in the normal force F_N between the first phase MEXICO experiment and the second phase new MEXICO experiment. Consistently higher normal force F_N is observed at $r/R = 0.82$ and 0.92. These differences mostly could be attributed to the improved calibration in the new MEXICO experiment. A significant normal force increase is observed at sections for the clean tip compared to the tripped tip, which further demonstrates that the ZigZag tape plays a significant role in affecting the tip loads. To be noted is that this ZigZag effect on sectional loads and chordwise pressure distribution can also be observed in the NREL Phase VI experiment, especially under low wind speeds with almost attached flow conditions, see the measured data with and without ZigZag in Figs. 3 and 5 of (Gomez-Iradi and Munduate, 2014).

Regarding the CFD results, the transitional and fully turbulent simulations are performed with the same conditions as in the experiments. Due to slightly different operating conditions between the MEXICO and new MEXICO experiments for the tripped configurations, small differences in the normal forces are observed from the corresponding fully turbulent simulation results. To be noted is that although the calibration and loads measurements in the new MEXICO experiment are considered to have much higher quality compared to the MEXICO experiment, the results of fully turbulent simulations still significantly overpredict the

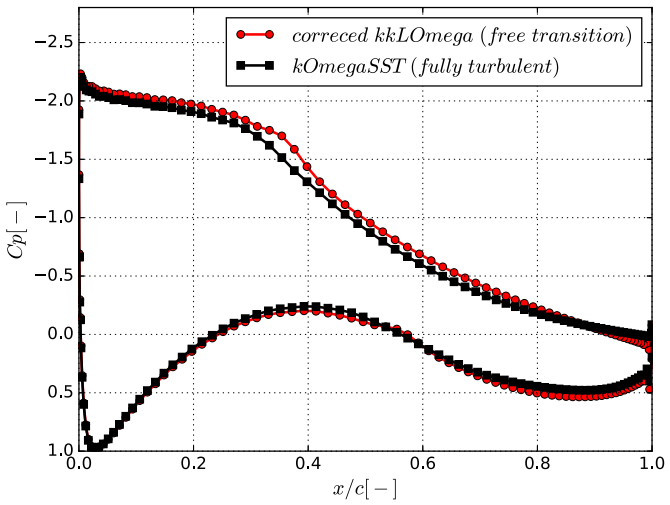

Fig. 18. C_p comparison between fully turbulent and transitional flow at $r/R = 0.35$ radial section ($\lambda = 6.7$, $U_\infty = 15.03m/s$, $n = 425.1rpm$, $\rho = 1.191kg/m^3$).

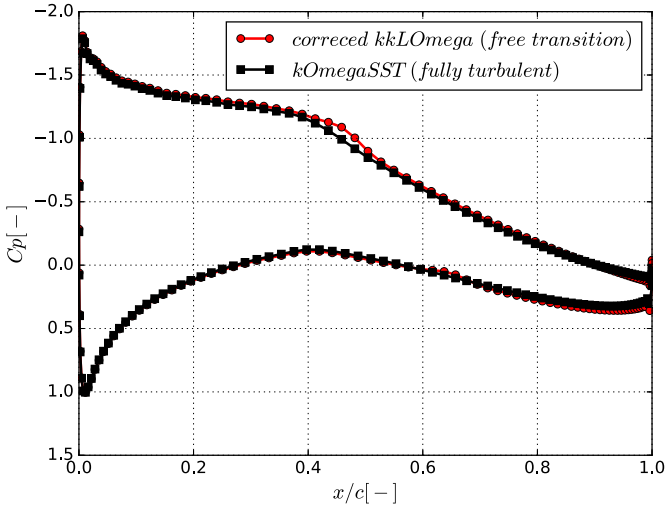

Fig. 19. C_p comparison between fully turbulent and transitional flow at $r/R = 0.92$ radial section ($\lambda = 6.7$, $U_\infty = 15.03m/s$, $n = 425.1rpm$, $\rho = 1.191kg/m^3$).

aerodynamic loads on the tripped blade at the tip. Again, the reason is that the ZigZag tape decreases the normal force further by performing more than tripping the boundary layer. By eliminating the ZigZag tape effects, the results of free transitional simulation considering laminar-turbulent boundary layer transition agrees very well with the experimental results.

Fig. 21 shows the comparison of tangential force along the blade between CFD and experiment. Only the pressure contribution is considered here and the viscous contribution is excluded in the tangential force, both for CFD and experiment. A higher tangential force is predicted at the tip by CFD compared to experimental data, for both clean and tripped conditions. The possible reason might be the limited resolution of chordwise pressure sensor lead to an underprediction of the measured tangential force.

5.4. Transition onset visualization

Fig. 22 shows the contour of turbulent kinetic energy k_t distribution in the first layer cells which are adjacent to the blade surface, which is used to identify the transition onset. The contour plot clearly shows that there is large portion of the flow still being laminar, both for the suction side and the pressure side. The transition line indicated by means of k_t

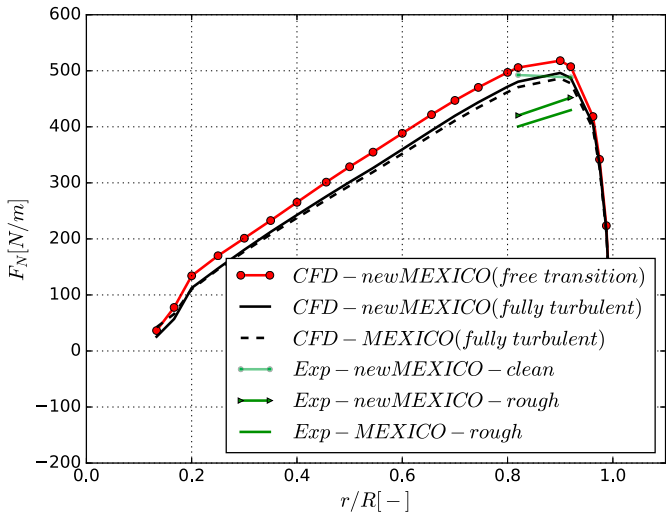

Fig. 20. Comparison of normal force distribution along the blade between numerical predictions and experimental measurements. Three different experimental conditions are MEXICO rough ($U_\infty = 14.93m/s$, $n = 424.5rpm$, $\rho = 1.246kg/m^3$), new MEXICO clean ($U_\infty = 15.03m/s$, $n = 425.1rpm$, $\rho = 1.191kg/m^3$) and new MEXICO rough ($U_\infty = 14.86m/s$, $n = 425.1rpm$, $\rho = 1.20kg/m^3$).

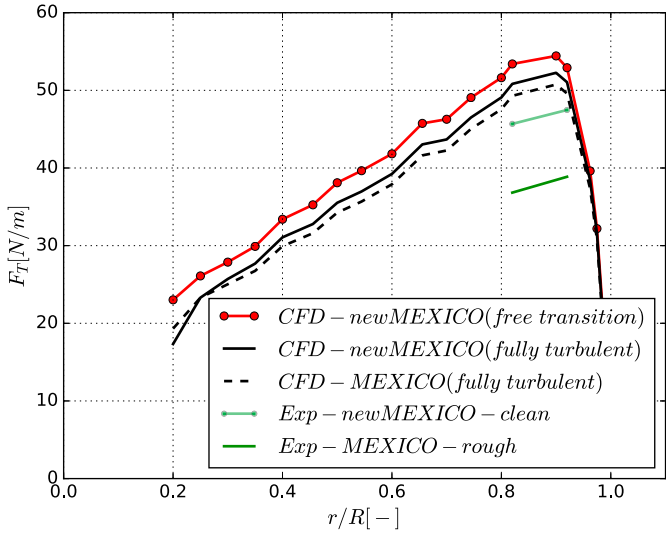

Fig. 21. Comparison of tangential force distribution along the blade between numerical predictions and experimental measurements. Three different experimental conditions are MEXICO rough ($U_\infty = 14.93m/s$, $n = 424.5rpm$, $\rho = 1.246kg/m^3$), new MEXICO clean ($U_\infty = 15.03m/s$, $n = 425.1rpm$, $\rho = 1.191kg/m^3$) and new MEXICO rough ($U_\infty = 14.86m/s$, $n = 425.1rpm$, $\rho = 1.20kg/m^3$).

distribution along the blade is similar as streaking patterns of the vector field wall shear stress by using line integral convolution (LIC) technique (Cabral and Leedom, 1993) in ParaView. More specifically, Fig. 23 quantifies the exact transition onset location $\frac{x_{tran}}{c}$ along the blade at $\lambda = 6.7$. Under this condition, transition from laminar to turbulent on the suction side occurs earlier than the pressure side. At the inboard part of the blade ($r/R < 0.60$), the locations of transition onset related to the local chord along the blade span have slight changes, while at the outboard part of the blade ($r/R > 0.60$), the transition location shows dramatic variations. The transition location moves closer to the trailing edge as the radius becomes larger.

6. Conclusions

This paper investigates the effects of ZigZag tape on sectional

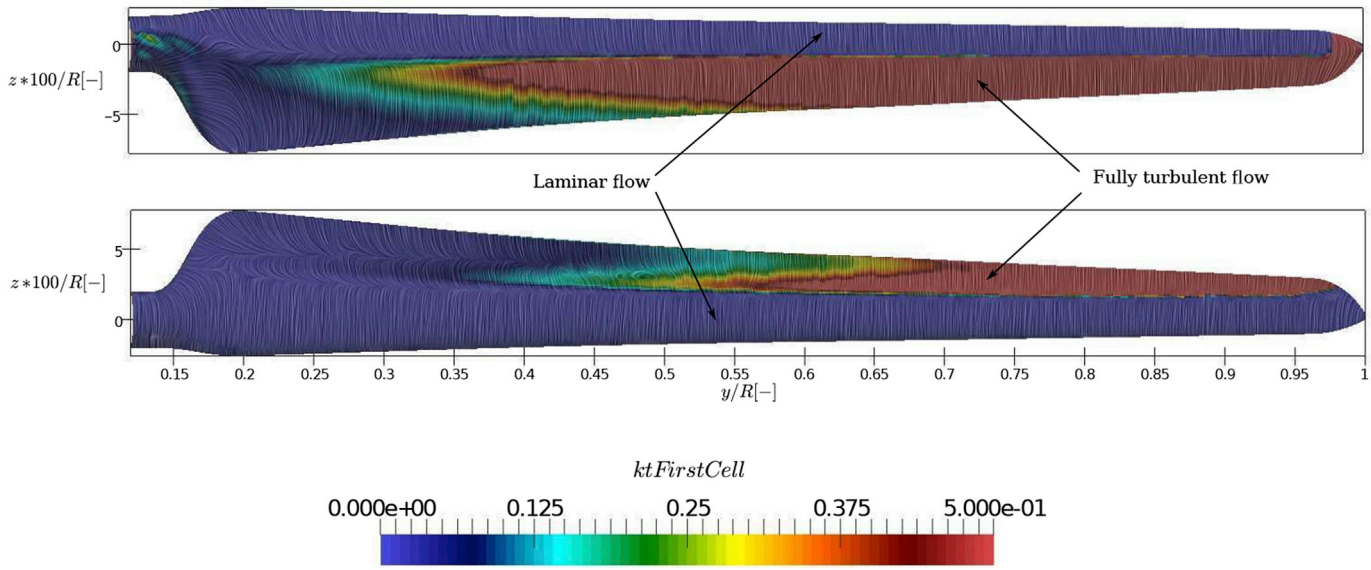

Fig. 22. Transition onset on the suction side (upper figure) and pressure side (lower figure) of the blade, overlap with LIC texture for wall shear stress in ParaView. The red color indicates the flow is fully turbulent. (For interpretation of the references to colour in this figure legend, the reader is referred to the web version of this article.)

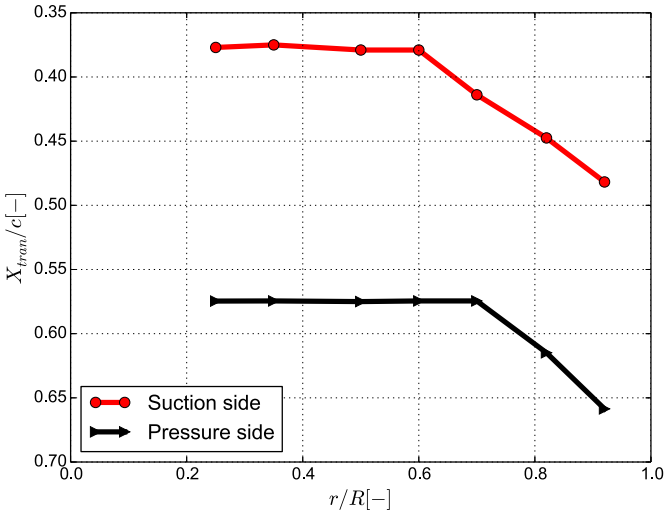

Fig. 23. Transition onset locations along the blade span at suction and pressure sides with optimal tip speed ratio $\lambda = 6.7$.

aerodynamic tip loads by the analysis of measured data in the non-rotating MEXICO experiment. In addition, a RANS-based 3D transitional flow simulation is performed for the MEXICO rotor in order to improve the tip loads prediction and quantitatively investigate the transitional effects. Some observations and conclusions can be summarized as:

- ZigZag tape has a significant impact on the aerodynamic characteristics for sectional airfoils of MEXICO blade. For the NACA airfoil at $r/R = 0.92$ radial location, ZigZag tape plays an important role in lift reduction at specific flow regimes: $\alpha = 4^{\circ} \sim 11^{\circ}$. Regarding the ZigZag tape effects on drag force, considerable drag increase occurs at $\alpha < 10^{\circ}$, but less influence on the drag when $\alpha > 10^{\circ}$.
- ZigZag tape performs much more than what is expected in tripping flow transition at specific locations in the experiment. It significantly alters the boundary layer displacement thickness and further the airfoil camber, which is a probable explanation why fully turbulent CFD result significantly overpredicts the normal force. Much closer sectional normal force agreement is obtained between the fully turbulent CFD result and the experimental data with clean blade configuration in the non-rotating MEXICO experiment.
- By eliminating the ZigZag tape interference in the new MEXICO experiment, very good agreement of aerodynamic loads on the clean blade tip is obtained between experimental results and 3D transitional flow simulation. The large difference in the measured normal force at the blade tip between clean and tripped conditions further confirms that ZigZag tape indeed has a significant influence on the blade tip loads in the rotating conditions.
- It can be concluded from the present study that ZigZag tape is the probable cause resulting large discrepancies between fully turbulent CFD results and measured tip loads on blade with ZigZag tape configuration observed in the blind MEXICO aerodynamic loads comparison.
- Under the design tip speed ratio $\lambda = 6.7$, large portion of the flow over the MEXICO blade is still laminar. Flow transition from laminar to turbulent occurs earlier on the suction side than on the pressure side. At the inboard part of blade ($r/R < 0.6$), the locations of transition onset related to the local chord are almost constant, but dramatically move toward to the trailing edge when the radial location increases.

Acknowledgements

The authors would like to acknowledge the MEXICO consortium which make the featured experiments possible. The financial support of China Scholarship Council (Grant no. 201206060043) is gratefully acknowledged. The OpenFOAM community and code developers is also acknowledged.

References

Bechmann, A., Sørensen, N.N., Zahle, F., 2011. Cfd simulations of the mexico rotor. Wind Energy 14 (5), 677–689.
Boorsma, K., Schepers, J., 2014. New Mexico Experiment, Preliminary Overview with Initial Validation. Tech. rep., Technical report. Energy Research Center of the Netherlands, ECN.
Boorsma, K., Schepers, J., 2015. Description of Experimental Setup, New Mexico Experiment. Tech. rep., Technical Report ECN-X15–093. ECN.
Braslow, A.L., Knox, E.C., 1958. Simplified Method for Determination of Critical Height of Distributed Roughness Particles for Boundary-layer Transition at Mach Numbers from 0 to 5. National Advisory Committee for Aeronautics.

Cabral, B., Leedom, L.C., 1993. Imaging vector fields using line integral convolution. In: Proceedings of the 20th Annual Conference on Computer Graphics and Interactive Techniques. ACM, pp. 263–270.
Farrell, P., Maddison, J., 2011. Conservative interpolation between volume meshes by local galerkin projection. Comput. Methods Appl. Mech. Eng. 200 (1), 89–100.
Fürst, J., Příhoda, J., Straka, P., 2013. Numerical simulation of transitional flows. Computing 95 (1), 163–182.
Gomez-Iradi, S., Munduate, X., 2014. Zig-zag tape influence in nrel phase vi wind turbine. In: Journal of Physics: Conference Series, vol. 524. IOP Publishing, p. 012096.
Hand, M.M., Simms, D., Fingersh, L., Jager, D., Cotrell, J., Schreck, S., Larwood, S., 2001. Unsteady Aerodynamics Experiment Phase VI: Wind Tunnel Test Configurations and Available Data Campaigns. National Renewable Energy Laboratory Golden, Colorado, USA.
Jasak, H., Error Analysis and Estimation for Finite Volume Method with Applications to Fluid Flow.
Menter, F., Esch, T., 2001. Elements of industrial heat transfer predictions. In: 16th Brazilian Congress of Mechanical Engineering (COBEM), pp. 26–30.
Moser, R.D., Kim, J., Mansour, N.N., 1999. Direct numerical simulation of turbulent channel flow up to re= 590. Phys. Fluids 11 (4), 943–945.
Patankar, S.V., Spalding, D.B., 1972. A calculation procedure for heat, mass and momentum transfer in three-dimensional parabolic flows. Int. J. Heat Mass Transf. 15 (10), 1787–1806.
Plaza, B., Bardera, R., Visiedo, S., 2015. Comparison of bem and cfd results for mexico rotor aerodynamics. J. Wind Eng. Ind. Aerodyn. 145, 115–122.
Rhie, C., Chow, W., 1983. Numerical study of the turbulent flow past an airfoil with trailing edge separation. AIAA J. 21 (11), 1525–1532.
Schepers, J., Boorsma, K., Cho, T., Gomez-Iradi, S., Schaffarczyk, P., Jeromin, A., Shen, W., Lutz, T., Meister, K., Stoevesandt, B., et al., 2014. Final report of iea task 29, mexnext (phase 1): analysis of mexico wind tunnel measurements. Wind Energy 2013, 2012.
Selig, M.S., 1995. Summary of Low Speed Airfoil Data, vol. 1. SoarTech.
Snel, H., Schepers, J., Montgomerie, B., 2007. The mexico project (model experiments in controlled conditions): the database and first results of data processing and interpretation. In: Journal of Physics: Conference Series, vol. 75. IOP Publishing, p. 012014.
Tsalicoglou, C., Jafari, S., Chokani, N., Abhari, R.S., 2014. Rans computations of mexico rotor in uniform and yawed inflow. J. Eng. Gas Turbines Power 136 (1), 011202.
Van Rooij, R., reportModification of the Boundary Layer Calculation in Rfoil for Improved Airfoil Stall Prediction, Report IW-96087R TU-Delft, The Netherlands.
Van Rooij, R., Timmer, W., 2003. Roughness sensitivity considerations for thick rotor blade airfoils. J. Sol. Energy Eng. 125 (4), 468–478.
Walters, D.K., Leylek, J.H., 2002. A new model for boundary-layer transition using a single-point rans approach. In: ASME 2002 International Mechanical Engineering Congress and Exposition. American Society of Mechanical Engineers, pp. 67–79.
Zhang, Y., van Zuijlen, A., van Bussel, G., 2014. Comparison of cfd simulations to non-rotating mexico blades experiment in the ltt wind tunnel of tudelft. In: Journal of Physics: Conference Series, vol. 524. IOP Publishing, p. 012013.
Zhang, Y., Gillebaart, T., Zuijlen, A., Bussel, G., Bijl, H., Experimental and numerical investigations of aerodynamic loads and 3d flow over non-rotating mexico blades. Wind Energy.